Bulletin of the Seismological Society of America, 89, 5, pp. 1156–1170, October 1999

SEA99: A Revised Ground Motion Prediction Relation for Use in Extensional Tectonic Regimes

by P. Spudich, W. B. Joyner, A. G. Lindh, D. M. Boore, B. M. Margaris, and J. B. Fletcher

Abstract We present SEA99, a revised predictive relation for geometric mean horizontal peak ground acceleration and 5%-damped pseudovelocity response spectrum, appropriate for estimating earthquake ground motions in extensional tectonic regimes, which we demonstrate to have lower ground motions than other tectonic regimes. SEA99 replaces SEA96, a relation originally derived by Spudich *et al.* (1996, 1997). The data set used to develop SEA99 is larger than that for SEA96, and minor errors in the SEA96 data set have been corrected. In addition, a one-step regression method described by Joyner and Boore (1993, 1994) was used rather than the two-step method of Joyner and Boore (1981). SEA99 has motions that are as much as 20% higher than those of SEA96 at short distances (5–30 km), and SEA99's motions are about 20% lower than SEA96 at longer periods (1.0–2.0 sec) and larger distance (40–100 km). SEA99 dispersions are significantly less than those of SEA96. SEA99 rock motions are on the average 20% lower than motions predicted by Boore *et al.* (1994) except for short distances at periods around 1.0 sec, where SEA99 motions exceed those predicted by Boore *et al.* (1994) by as much as 10%. Comparison of ground motions from normal-faulting and strike-slip events in our data set indicates that normal-faulting horizontal ground motions are not significantly different from extensional regime strike-slip ground motions.

Introduction

We present SEA99, a revised predictive relation for horizontal peak ground acceleration and 5%-damped pseudovelocity response (PSV) spectrum, appropriate for estimating earthquake ground motions in extensional tectonic regimes. SEA99 replaces SEA96, a relation originally derived by Spudich *et al.* (1996, 1997) as part of a project to estimate seismic hazard at the site of a proposed nuclear waste repository at Yucca Mountain, Nevada, which is located in the Basin and Range province of the western U.S., an extensional regime. We have numerous reasons for updating SEA96. First, we have enlarged the data set, adding data from a larger range of magnitudes and distances. Consequently we have extended the maximum distance of applicability of SEA99 to 100 km. Second, we have corrected minor errors in the SEA96 data set. Third, we developed the regression coefficients by using the one-step regression method described by Joyner and Boore (1993, 1994) rather than the two-step method of Joyner and Boore (1981). Fourth, we decided to use the soil coefficient determined by Boore *et al.* (1997) rather than obtaining one from our data set. Finally, in this article, we can more completely document the development and validation of SEA99. The motives for developing SEA99 are discussed in more detail subsequently.

In this study, we use the same data selection criteria as used by Spudich *et al.* (1996, 1997), which we summarize very briefly here. Those references should be consulted for more details. We developed our relation based on data from extensional regime earthquakes having moment magnitude $\mathbf{M} \geq 5.0$ recorded at distances less than 105 km. Extensional regions are regions in which the lithosphere is expanding areally. There are three reasons for restricting our attention to ground-motion data from earthquakes in extensional provinces. First, there is observational evidence that the state of stress, extensional or compressional, affects the amplitude of the ground motion from an earthquake (McGarr, 1984; Abrahamson and Silva, 1997). McGarr (1984) suggested that extensional regime events have lower motions than events in other stress regimes. Second, the theoretical study of Oglesby *et al.* (1998) and the lab study of Brune and Anooshehpoor (1999) show differences in ground motion caused by differences in source mechanism. A third way in which the stress state might affect the recorded ground motion involves possible differences in wave-propagation characteristics between extensional and compressional tectonic regimes, owing to the typically higher heat flow, thinner crust, and higher velocity gradients in these regions (Chris-

tensen and Mooney, 1995). The extensional regions from which we obtained data are listed in Spudich *et al.* (1997).

In this study, we used only records that were available digitally. We obtained the uncorrected digitized records from the data source and we sent them to a contractor (W. Silva, Pacific Engineering and Analysis, El Cerrito, CA), who corrected and processed them. The procedure consisted of eight steps (1) interpolation of the uncorrected time series to 400 samples/sec, (2) low-pass filtering using a causal 5-pole butterworth filter with a corner frequency f_l selected for each record based on visual examination of the Fourier amplitude spectrum, (3) decimation to 100 or 200 samples/sec depending on the low-pass filter corner, (4) removal of the instrument response using instrument constants provided by each data source, (5) examination of the Fourier amplitude spectrum of each record to choose a high-pass filter corner f_h and to assess the adequacy of the low-pass anti-alias filter, (6) high-pass filtering of the accelerations with a causal 5-pole butterworth filter, (7) frequency-domain integration to velocity and displacement to evaluate low-frequency noise levels (baseline drifts) in the time domain, and (8) either baseline correction or refiltering if the low-frequency noise is minor or severe, respectively. The baseline correction procedure fit a polynomial (typically of degree 5) to the displacement-time history and subtracted its second derivative from the acceleration record. Response spectra were calculated from the filtered, corrected time series. In our regression, we only used response spectral data within the band 1.25 f_h to 0.75 f_l in order to avoid the effects of the filter roll-off near the corner frequencies. All data were processed as described above except those from the 29 June 1992 Little Skull Mountain earthquake, for which we have only the processed data supplied by URS/Blume (Lum and Honda, undated). Because we do not know the instrument constants or the low- and high-frequency corners used in the URS processing, we have used the horizontal data only for peak acceleration and response spectra in the 0.1 to 1.0 sec band.

We rejected records from structures of more than two stories in height, from deeply embedded basements, or from instruments that triggered during the *S* wave. For each earthquake, we retained records recorded at distances greater than the cutoff distance, which is the distance beyond the first untriggered accelerograph. Some authors (e.g., Boore *et al.*, 1997) do not use records recorded at distances greater than the cutoff distance because these motions may be biased systematically high. However, we decided to retain these records because of the relatively small number of records available to us and the difficulty of determining the existence of nontriggered accelerographs for some earthquakes.

Recording sites were classified into two geologic categories, rock and soil, following the classification scheme of Joyner and Boore (1981), which will be described in more detail subsequently. We used the source-receiver distance metric of Joyner and Boore (1981, 1988), the shortest distance from the receiver to the vertical projection onto the Earth's surface of the fault rupture area. The fault rupture area was determined as described in Spudich *et al.* (1997).

Data Set

Table 1 lists the records used to develop SEA99, and Figures 1 and 2 show the magnitude–distance distribution of data used in SEA99 and SEA96. The SEA99 data set differs in several ways from that used to develop SEA96.

First, several new events were added, namely the 1995, M 6.6 Kozani, Greece, earthquake (also sometimes known as the Grevena earthquake) and its aftershocks (Papazachos *et al.*, 1995; Clarke *et al.*, 1997), the 1995 M 6.40 Dinar, Turkey, earthquake (Erdik and Durukal, 1997; Durukal *et al.*, 1998), the 1995 M 7.20 Gulf of Aqaba (Nuweiba) earthquake (Shamir, 1996; Hillel, 1997), the 1981 M 6.6 Corinth, Greece, earthquake, the 1990 M 6.1 Griva, Greece, earthquake, and the 1985 M 5.2 Drama, Greece, earthquake. The Gulf of Aqaba event is notable for being the largest event of our data set, and the Dinar and Kozani events were fairly well recorded. The general effect of the new data was to add data at the high and low magnitude ends of the distribution and to add data at zero distance and at large distances (Fig. 1 and 2). Because we have added data from both large and small magnitude events at distances greater than 70 km, we feel warranted in extending the maximum range of applicability of SEA99 to 100 km, rather than the 70 km of SEA96.

Second, a number of source-receiver distances changed because of correction of incorrect fault or station locations, and a few site geologies and magnitudes were revised. Specifically, we shifted and extended our assumed fault plane of the 23 November 1980, 1834 Irpinia main shock in order to match more closely the northwest extent of the fault plane used by Cocco and Pacor (1993). The most important consequence of this correction was to change the distance to station Sturno from 16.2 to 6.7 km. Distances to other stations changed by 7 km or less. We fixed an error in the location of Irpinia station Bisaccia, which changed the distance to the main shock fault by about 5 km and to the aftershock (23 November 1980, 1835) by about 8 km. We revised the magnitude of the Irpinia main shock from 6.90 to 6.87 to remove the contribution of the 1835 event (the 40-sec subevent), which had been incorrectly included in the SEA96 magnitude. An error in the location of the 7 May 1984, 1749 Lazio-Abruzzo source was fixed, and station Atina coordinates were corrected, causing distance revisions as large as 11 km. Site geology of the 7 May 1984 earthquake station Roccamonfina was revised to rock. The locations of the 6 August 1983 North Aegean Sea source and the 2 March 1987 0150 Edgecumbe, New Zealand aftershock were improved, causing a 5-km and 10-km distance change, respectively. The location of the 13 March 1992 Erzincan source was revised according to new information from Fuenzalida *et al.* (1997).

Third, stations were added to or deleted from the data

Table 1
Records, Parameters, and Data Sources Used to Develop SEA99

Date (yy.mm.dd)	Time	Event	M	Rake	G	r_{jb}	r_{seis}	r_{run}	Station	Data Source*
40.05.19	05:36	Imperial Valley, CA	6.87	180	6	6.3	7.6	6.3	El Centro Array Sta 9	USGS
72.12.23	06:29	Managua, Nicaragua	6.20	−99	6	3.5	4.8	4.1	Managua: ESSO Refinery	USGS
79.09.19	21:35	Valnerina, Italy	5.90	?	0	4.3	7.4	7.4	Cascia	ENEL
79.09.19	21:35	Valnerina, Italy	5.90	?	6	36.0	36.5	36.5	Bevagna	ENEL
79.09.19	21:35	Valnerina, Italy	5.90	?	6	18.3	19.2	19.2	Spoleto	ENEL
79.10.15	23:16	Imperial Valley, CA	6.50	180	2	24.5	25.0	24.5	Superstition Mtn	USGS
79.10.15	23:16	Imperial Valley, CA	6.50	180	6	8.6	9.7	8.6	El Centro Array Sta 10	USGS
79.10.15	23:16	Imperial Valley, CA	6.50	180	6	35.4	36.7	36.7	Niland	CSMIP
79.10.15	23:16	Imperial Valley, CA	6.50	180	6	1.0	3.2	1.0	El Centro Array Sta 5	USGS
79.10.15	23:16	Imperial Valley, CA	6.50	180	6	4.2	5.2	4.2	El Centro Array Sta 4	USGS
79.10.15	23:16	Imperial Valley, CA	6.50	180	6	0.6	3.4	0.6	El Centro Array Sta 7	USGS
79.10.15	23:16	Imperial Valley, CA	6.50	180	6	12.5	13.3	12.5	Parachute Test Site	USGS
79.10.15	23:16	Imperial Valley, CA	6.50	180	6	10.4	11.4	10.4	Calexico	USGS
79.10.15	23:16	Imperial Valley, CA	6.50	180	6	0.4	3.8	2.7	Bonds Corner	USGS
79.10.15	23:16	Imperial Valley, CA	6.50	180	6	5.5	7.8	7.6	Holtville	USGS
79.10.15	23:16	Imperial Valley, CA	6.50	180	6	15.9	16.2	15.9	El Centro Array Sta 1	USGS
79.10.15	23:16	Imperial Valley, CA	6.50	180	6	9.1	9.6	9.1	El Centro Array Sta 3	USGS
79.10.15	23:16	Imperial Valley, CA	6.50	180	6	12.5	13.4	12.5	El Centro Array Sta 11	USGS
79.10.15	23:16	Imperial Valley, CA	6.50	180	6	22.0	22.8	22.0	El Centrol Array Sta 13	USGS
79.10.15	23:16	Imperial Valley, CA	6.50	180	6	8.4	10.3	9.9	Brawley	USGS
79.10.15	23:16	Imperial Valley, CA	6.50	180	6	23.3	24.7	24.7	Calipatria	USGS
79.10.15	23:16	Imperial Valley, CA	6.50	180	6	48.8	49.8	49.8	Coachella Canal Sta 4	USGS
79.10.15	23:16	Imperial Valley, CA	6.50	180	6	10.4	10.9	10.4	El Centro Array Sta 2	USGS
79.10.15	23:16	Imperial Valley, CA	6.50	180	6	7.4	8.5	7.4	El Centro: Imp. Cnty Cntr FF	CSMIP
79.10.15	23:16	Imperial Valley, CA	6.50	180	6	0.0	3.2	0.1	El Centro: Meloland Overpass	CSMIP
79.10.15	23:16	Imperial Valley, CA	6.50	180	6	0.0	3.1	0.9	El Centro Arry Sta 6	USGS
79.10.15	23:16	Imperial Valley, CA	6.50	180	6	3.9	5.5	3.9	El Centro Arry Sta 8	USGS
79.10.15	23:16	Imperial Valley, CA	6.50	180	6	5.2	6.5	5.2	El Centro: Differential Array	USGS
79.10.15	23:16	Imperial Valley, CA	6.50	180	6	14.6	15.3	15.1	Westmorland	CSMIP
79.10.15	23:16	Imperial Valley, CA	6.50	180	6	18.0	18.8	18.0	El Centro Array Station 12	USGS
79.10.15	23:16	Imperial Valley, CA	6.50	180	6	0.0	3.2	0.4	Aeropuerto	UNAM
79.10.15	23:16	Imperial Valley, CA	6.50	180	6	0.0	3.2	0.7	Agrarias	UNAM
79.10.15	23:16	Imperial Valley, CA	6.50	180	2	15.2	16.0	15.2	Cerro Prieto	UNAM
79.10.15	23:16	Imperial Valley, CA	6.50	180	6	7.2	8.2	7.2	Chihuahua	UNAM
79.10.15	23:16	Imperial Valley, CA	6.50	180	6	13.5	15.3	15.3	Compuertas	UNAM
79.10.15	23:16	Imperial Valley, CA	6.50	180	6	1.0	3.3	1.1	Cucapah	UNAM
79.10.15	23:16	Imperial Valley, CA	6.50	180	6	21.9	22.4	21.9	Delta	UNAM
79.10.15	23:16	Imperial Valley, CA	6.50	180	6	31.8	32.1	31.8	Victoria	UNAM
80.05.25	16:33	Mammoth Lakes, CA ev I	6.20	−35	6	1.1	6.6	6.6	Convict Creek	CSMIP
80.05.25	16:33	Mammoth Lakes, CA ev I	6.20	−35	6	4.5	6.6	4.7	Mammoth Lakes H.S. gym	CSMIP
80.05.25	16:49	Mammoth Lakes, CA ev J	5.80	0	6	2.9	9.5	9.5	Convict Creek	CSMIP
80.05.25	16:49	Mammoth Lakes, CA ev J	5.80	0	6	3.5	9.7	9.7	Mammoth Lakes H.S. gym	CSMIP
80.05.25	19:44	Mammoth Lakes, CA ev A	5.80	−11	6	1.7	10.6	10.6	Convict Creek	CSMIP
80.05.25	19:44	Mammoth Lakes, CA ev A	5.80	−11	1	10.1	18.0	18.0	Long Valley Dam CRA 11-13	CSMIP
80.05.25	20:35	Mammoth Lakes, CA ev B	5.70	?	6	2.8	5.7	5.7	Convict Creek	CSMIP
80.05.25	20:35	Mammoth Lakes, CA ev B	5.70	?	1	14.2	15.1	15.1	Long Valley Dam CRA 11-13	CSMIP
80.05.27	14:50	Mammoth Lakes, CA ev L	6.00	−28	5	41.0	43.3	43.3	Bishop Paradise Lodge	CSMIP
80.05.27	14:50	Mammoth Lakes, CA ev L	6.00	−28	6	5.9	9.3	9.3	Convict Creek	CSMIP
80.05.27	14:50	Mammoth Lakes, CA ev L	6.00	−28	5	41.8	44.1	44.1	Benton	CSMIP
80.05.27	14:50	Mammoth Lakes, CA ev L	6.00	−28	5	6.0	9.3	9.3	Fish and Game	CSMIP
80.06.09	03:28	Victoria, Mexico	6.32	0	6	25.1	25.4	25.4	Cucapah	UNAM
80.06.09	03:28	Victoria, Mexico	6.32	0	6	38.6	38.8	38.8	Mexicali SAHOP	UNAM
80.11.23	18:34	Irpinia, Italy	6.87	−90	2	17.5	21.2	21.2	Bisaccia	ENEL
80.11.23	18:34	Irpinia, Italy	6.87	−90	6	44.6	46.2	46.2	Bovino	ENEL
80.11.23	18:34	Irpinia, Italy	6.87	−90	2	13.3	17.6	17.6	Calitri	ENEL
80.11.23	18:34	Irpinia, Italy	6.87	−90	6	30.1	32.3	30.1	Mercato San Severino	ENEL
80.11.23	18:34	Irpinia, Italy	6.87	−90	2	27.5	30.1	30.1	Rionero in Vulture	ENEL
80.11.23	18:34	Irpinia, Italy	6.87	−90	2	6.7	10.7	10.7	Sturno	ENEL
80.11.23	18:34	Irpinia, Italy	6.87	−90	1	60.1	62.0	60.1	Torre del Greco	ENEL

(*continued*)

Table 1
Continued

Date (yy.mm.dd)	Time	Event	M	Rake	G	r_{ib}	r_{seis}	r_{run}	Station	Data Source*
80.11.23	18:34	Irpinia, Italy	6.87	−90	0	53.4	54.6	53.4	Arienzo	ENEL
80.11.23	18:34	Irpinia, Italy	6.87	−90	0	8.3	10.9	8.3	Bagnoli Irpinio	ENEL
80.11.23	18:35	Irpinia, Italy AS	6.20	−90	2	28.9	30.0	30.0	Auletta	ENEL
80.11.23	18:35	Irpinia, Italy AS	6.20	−90	2	14.3	16.0	14.3	Bisaccia	ENEL
80.11.23	18:35	Irpinia, Italy AS	6.20	−90	6	43.0	44.5	43.0	Bovino	ENEL
80.11.23	18:35	Irpinia, Italy AS	6.20	−90	6	41.9	42.8	42.8	Brienza	ENEL
80.11.23	18:35	Irpinia, Italy AS	6.20	−90	2	8.4	10.3	8.4	Calitri	ENEL
80.11.23	18:35	Irpinia, Italy AS	6.20	−90	6	43.9	44.8	44.8	Mercato San Severino	ENEL
80.11.23	18:35	Irpinia, Italy AS	6.20	−90	2	22.3	23.8	22.3	Rionero in Vulture	ENEL
80.11.23	18:35	Irpinia, Italy AS	6.20	−90	2	20.3	20.8	20.3	Sturno	ENEL
80.11.23	18:35	Irpinia, Italy AS	6.20	−90	6	64.4	64.8	64.4	Tricarico	ENEL
80.11.23	18:35	Irpinia, Italy AS	6.20	−90	0	18.2	19.9	19.9	Bagnoli Irpinio	ENEL
81.02.24	20:53	Corinth, Greece	6.60	−60	6	10.2	13.8	10.2	Corinth	ITSAK
81.04.26	12:09	Westmoreland, CA	5.90	0	2	19.1	19.3	19.2	Superstition Mtn	USGS
81.04.26	12:09	Westmoreland, CA	5.90	0	6	15.1	15.4	15.3	Niland	CSMIP
81.04.26	12:09	Westmoreland, CA	5.90	0	6	16.5	16.7	16.6	Parachute Test Site	USGS
81.04.26	12:09	Westmoreland, CA	5.90	0	6	15.3	15.6	15.4	Brawley	USGS
81.04.26	12:09	Westmoreland, CA	5.90	0	6	8.0	8.5	8.2	Salton Sea Wildlife Refuge	USGS
81.04.26	12:09	Westmoreland, CA	5.90	0	6	6.2	6.8	6.5	Westmorland	CSMIP
83.08.06	15:43	North Aegean Sea, Greece	6.74	−179	5	76.4	76.9	76.4	Ierissos	ITSAK
83.10.28	14:06	Borah Peak, ID	6.90	−70	7	83.1	84.2	83.1	CPP-610	INEL
83.10.28	14:06	Borah Peak, ID	6.90	−70	7	84.9	86.9	84.9	TAN-719	INEL
83.10.29	23:29	Borah Peak AS, ID	5.10	−65	5	16.9	19.4	19.4	BOR	USGS
83.10.29	23:29	Borah Peak AS, ID	5.10	−65	2	22.0	23.9	23.9	CEM	USGS
83.10.29	23:29	Borah Peak AS, ID	5.10	−65	1	49.3	50.2	50.2	HAU	USGS
84.05.07	17:49	Lazio-Abruzzo, Italy	5.80	−96	0	12.9	18.9	18.9	Atina	ENEL
84.05.07	17:49	Lazio-Abruzzo, Italy	5.80	−96	6	29.7	31.2	31.2	Isernia-Satn'agapito	ENEL
84.05.07	1749	Lazio-Abruzzo, Italy	5.80	−96	6	49.3	51.3	51.3	Garigliano-Centrale Nucleare	ENEL
84.05.07	17:49	Lazio-Abruzzo, Italy	5.80	−96	6	29.7	32.8	32.8	Pontecorvo	ENEL
84.05.07	17:49	Lazio-Abruzzo, Italy	5.80	−96	0	45.5	47.5	47.5	Roccamonfina	ENEL
85.11.09	23:30	Drama, Greece	5.20	−121	1	43.4	44.5	43.4	Kavala, Greece	ITSAK
86.07.20	14:29	Chalfant Valley, CA FS B	5.80	20	5	17.5	18.2	17.5	Bishop-LADWP	CSMIP
86.07.20	14:29	Chalfant Valley, CA FS B	5.80	20	5	25.0	26.0	26.0	Benton	CSMIP
86.07.20	14:29	Chalfant Valley, CA FS B	5.80	20	2	14.0	15.3	15.3	Bishop Paradise Lodge	CSMIP
86.07.20	14:29	Chalfant Valley, CA FS B	5.80	20	5	7.4	8.4	8.1	Chalfant–Zack Ranch	CSMIP
86.07.20	14:29	Chalfant Valley, CA FS B	5.80	20	5	25.2	26.5	26.5	Crowley Lake	CSMIP
86.07.21	14:42	Chalfant Valley, CA	6.30	−160	5	19.4	21.3	21.3	Bishop-LADWP	CSMIP
86.07.21	14:42	Chalfant Valley, CA	6.30	−160	6	31.8	33.3	33.3	Convict Creek	CSMIP
86.07.21	14:42	Chalfant Valley, CA	6.30	−160	5	20.3	20.7	20.7	Benton	CSMIP
86.07.21	14:42	Chalfant Valley, CA	6.30	−160	5	4.4	6.0	6.0	Chalfant–Zack Ranch	CSMIP
86.07.21	14:42	Chalfant Valley, CA	6.30	−160	6	28.7	30.4	30.4	McGee Creek	USGS
86.07.21	14:42	Chalfant Valley, CA	6.30	−160	5	24.7	26.6	26.6	Crowley Lake	CSMIP
86.07.21	14:42	Chalfant Valley, CA	6.30	−160	1	37.2	38.5	38.5	Mammoth Lakes Sheriff Substn.	CSMIP
86.07.21	14:42	Chalfant Valley, Ca	6.30	−160	1	21.0	23.2	23.2	Long Valley Dam CRA 11-13	CSMIP
86.07.21	14:42	Chalfant Valley, CA	6.30	−160	1	56.8	57.6	57.6	Tinemaha Reservoir FF	CSMIP
86.07.21	14:51	Chalfant Valley, CA AS C	5.60	?	5	24.9	25.4	25.4	Bishop-LADWP	CSMIP
86.07.21	14:51	Chalfant Valley, CA AS C	5.60	?	2	11.9	12.9	12.9	Bishop Paradise Lodge	CSMIP
86.07.21	14:51	Chalfant Valley, CA AS C	5.60	?	5	15.2	16.0	16.0	Chalfant–Zack Ranch	CSMIP
86.07.31	07:22	Chalfant Valley, CA AS D	5.80	160	5	22.1	22.3	22.2	Bishop-LADWP	CSMIP
86.07.31	07:22	Chalfant Valley, CA AS D	5.80	160	5	8.7	9.3	9.0	Chalfant–Zack Ranch	CSMIP
86.10.10	17:49	San Salvador, El Salvador	5.76	0	6	3.7	7.0	7.0	IGN, San Salvador	CSMIP
86.10.10	17:49	San Salvador, El Salvador	5.76	0	6	2.1	6.3	6.3	CIG, San Salvador	CSMIP
87.03.02	01:42	Edgecumbe MS, NZ	6.60	−110	7	18.9	20.1	19.1	Matahina Dam	IGNS
87.03.02	01:42	Edgecumbe MS, NZ	6.60	−110	7	70.1	70.6	70.2	Maraenui ES	IGNS
87.03.02	01:50	Edgecumbe AS, NZ	5.80	?	7	23.6	29.7	29.7	Matahina Dam	IGNS
87.11.24	01:54	Elmore Ranch, CA	6.20	180	6	19.8	20.0	19.8	Imperial Wildlife	USGS
87.11.24	13.15	Superstition Hills, CA	6.60	178	6	18.2	18.7	18.7	El Centro: Imp. Cnty Cntr FF	CSMIP
87.11.24	13:15	Superstition Hills, CA	6.60	178	6	13.1	13.7	13.7	Westmorland	CSMIP
90.12.21	06:57	Griva, Greece	6.10	−103	6	31.0	31.8	31.8	Kilkis	ITSAK
92.03.13	17:18	Erzincan, Turkey	6.70	−163	6	0.0	3.7	3.3	Erzincan	TNSMN

(*continued*)

Table 1
Continued

Date (yy.mm.dd)	Time	Event	M	Rake	G	r_{jb}	r_{seis}	r_{run}	Station	Data Source*
92.04.13	01:20	Roermond, Netherlands	5.31	−94	1	55.8	58.1	58.1	GSH	GLA
92.06.29	10:14	Little Skull Mt., NV	5.70	−70	6	14.1	16.1	16.1	Lathrop-A	URS
92.06.29	10:14	Little Skull Mt., NV	5.70	−70	1	23.8	24.6	24.6	NTS C.P.1 A	URS
92.06.29	10:14	Little Skull Mt., NV	5.70	−70	0	45.2	45.6	45.6	Beatty	URS
92.06.29	10:14	Little Skull, Mt., NV	5.70	−70	6	58.6	59.8	59.8	Pahrump 2	URS
92.06.29	10:14	Little Skull Mt., NV	5.70	−70	6	63.7	64.8	64.8	Pahrump 1	URS
92.06.29	10:14	Little Skull Mt., NV	5.70	−70	2	99.4	100.1	100.1	Calico Basin	URS
92.06.29	1014	Little Skull Mt., NV	5.70	−70	6	98.9	99.6	99.6	Ann Road	URS
92.06.29	10:14	Little Skull Mt., NV	5.70	−70	0	98.2	98.4	98.4	Scottie's Castle	URS
94.09.12	12:23	Double Spring Flat, NV	5.90	−25	6	12.5	12.9	12.9	Woodfords	CSMIP
95.05.13	08:47	Kozani, Greece	6.60	−95	1	11.4	17.7	17.7	Kozani	ITSAK
95.05.13	08:47	Kozani, Greece	6.60	−95	5	82.4	82.4	82.4	Kardista	ITSAK
95.05.13	08:47	Kozani, Greece	6.60	−95	1	44.3	46.4	46.4	Kastoria	ITSAK
95.05.15	04:13	Kozani, Greece, AS A	5.10	?	7	12.9	15.6	15.6	Chromio Anapasiktiri	ITSAK
95.05.15	04:13	Kozani, Greece, AS A	5.10	?	5	80.9	81.4	81.4	Grevena	ITSAK
95.05.17	04:14	Kozani, Greece, AS B	5.30	?	7	10.8	12.1	12.1	Chromio Anapasiktiri	ITSAK
95.05.17	04:14	Kozani, Greece, AS B	5.30	?	5	82.5	82.7	82.7	Grevena	ITSAK
95.05.19	06:48	Kozani, Greece, AS C	5.10	?	5	83.9	84.2	84.2	Grevena	ITSAK
95.05.19	06:48	Kozani, Greece, AS C	5.10	?	7	11.8	13.6	13.6	Karpero	ITSAK
95.10.01	15:57	Dinar, Turkey	6.40	−94	6	0.0	3.4	3.1	Dinar Meteoroloji Istasyonu	TNSMN
95.10.01	15:57	Dinar, Turkey	6.40	−94	6	34.7	37.7	37.7	Burdur Meteoroloji Istasyonu	TNSMN
95.10.01	15:57	Dinar, Turkey	6.40	−94	6	36.9	39.8	39.8	Cardak Saglik Ocagi	TNSMN
95.11.22	04:15	Gulf of Aqaba	7.20	7	6	43.3	43.6	43.3	Eilat	IPRG

*Institution Abbreviations: CSMIP, California Strong Motion Instrumentation Program; ENEL, Italian National Electric Utility; GLA, Geological Survey of North Rhine-Westfalia; IGNS, Institute of Geological and Nuclear Science, New Zealand; INEL, Idaho National Engineering Laboratory; IPRG, Inst. for Petroleum Research, Israel; ITSAK, Inst. of Engineering Seismology and Earthquake Engineering, Greece; TNSMN, Turkish National Strong Motion Network; UNAM, Univ. Nacional Autonomo de Mexico in cooperation with the Univ. of California at San Diego; URS, URS/John A. Blume and Associates, San Francisco, USA; USGS, U.S. Geological Survey.

set as more information became available. Station Spoleto was added to the 19 September 1979 Valnerina, Italy, earthquake. Station Bishop Paradise Lodge was removed for the 21 July 1986, 1442 Chafant Valley event because it was an *S* trigger. Stations OLF and WBS were removed from the data set for the 13 April 1992 Roermond earthquake because these stations were in or near very large dams, and we were not confident that the station responses were uncontaminated by structural response.

Fourth, we fixed a gain error of a factor of 10 in the data for station TAN-719 that recorded the 1983 M 6.9 Borah Peak, Idaho, earthquake. This change corrected the largest residual in the SEA96 data set.

One of the most important simplifications in our study is that in order to produce SEA99 we classified surficial geology at each recording site as either rock or soil. It would have been preferable to classify sites according to the shear-wave velocity in the top 30 m, as has been done by Boore *et al.* (1993, 1997). However, shear-velocity information was not available for many recording sites, and we wanted to use a method for describing site geologies that we could apply uniformly and would be broadly applicable. Hence, we adhered to a simple rock/soil categorization. However, Table 1 lists site geology in a more detailed breakdown using a categorization employed in Spudich *et al.* (1996), which we present here because this more detailed information might be useful to the reader. That categorization used the following categories. Hard rock ($G = 1$) included plutonic igneous rocks, lava flows, welded tuffs, and metamorphic rocks, unless these rocks are severely weathered, in which case they were considered soft rocks. Soft rocks ($G = 2$) included all sedimentary rocks unless there was some special characteristic noted in their description, such as crystalline limestone or massive cliff-forming sandstone, in which case they were considered hard rocks. If insufficient information was available to discriminate between hard and soft, we identified a site as unknown rock ($G = 0$). Sites described as alluvium, sand, gravel, clay, silt, mud, fill, or glacial outwash were considered soil sites, and if the soil was between 5-m and 20-m thick, the site was classified as shallow soil ($G = 7$). If the soil was more than 20-m thick, the site was classified as deep soil ($G = 6$). If soil depth was less than 5-m thick, the site was assigned the appropriate rock categorization, and if soil depth was unknown we used $G = 5$. For the development of SEA99, sites in Table 1 with G equal to 0, 1, or 2 were placed in the rock class, and sites with G equal to 5, 6, or 7 were placed in the soil class.

Although we used only the Joyner–Boore distance in this work, we calculated several other commonly used distance measures, and we present them in Table 1 for the con-

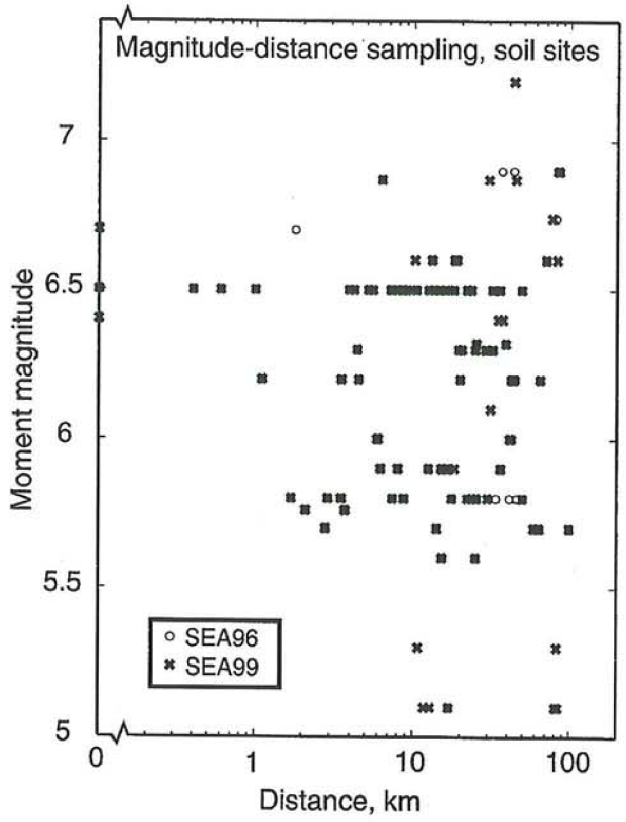

Figure 1. Magnitude–distance sampling for SEA99 (× symbols) and SEA96 (circles) for soil sites.

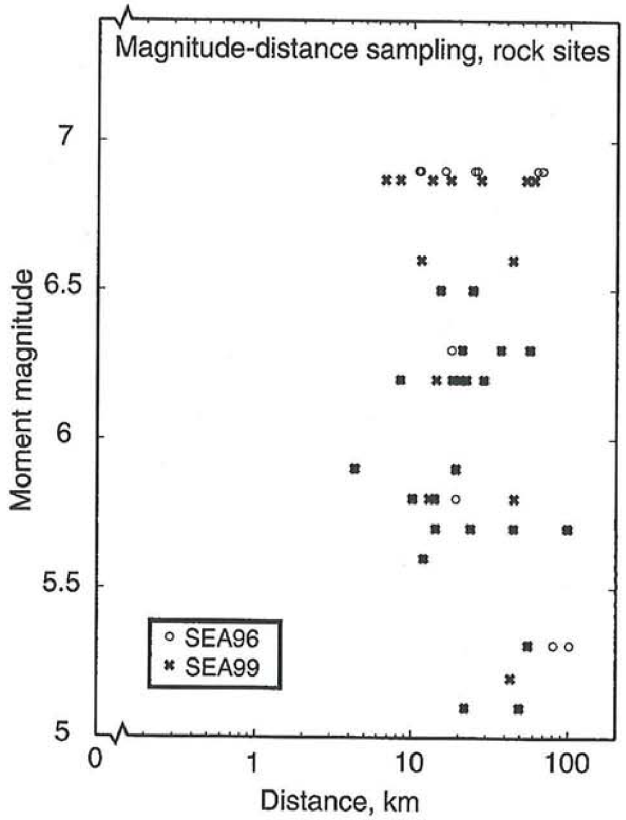

Figure 2. Magnitude–distance sampling for SEA99 (× symbols) and SEA96 (circles) for rock sites.

venience of the reader. Abrahamson and Shedlock (1997) give a clear explanation of the Joyner–Boore distance, r_{jb} the seismogenic distance r_{seis}, and the rupture distance r_{rup}. In our calculation of the seismogenic distance, we assumed the seismogenic depth was 3.0 km (see Abrahamson and Shedlock, 1997, Figure 1).

Extensional Regime Ground Motions Are Smaller

We use a more sophisticated statistical test to verify the crude result of Spudich *et al.* (1996) that extensional regime ground motions are smaller than ground motions in other tectonic regimes. To demonstrate this result, we show that the strike-slip predictive relation of Boore *et al.* (1997) systematically overpredicts our extensional regime data. Although some extensional regime data (most significantly from the 1979 Imperial Valley earthquake) were used to develop Boore's relation, we choose this relation as our example of nonextensional strike-slip ground motions because it was developed using less extensional regime data than were the relations of Abrahamson and Silva (1997) and Sadigh *et al.* (1997), and Boore's relation does not need the depth-to-basement information required by Campbell (1997).

Specifically, we define a residual to be

$$Y_{ei} = \log_{10}(y_{ei}) - \log_{10}(Z_{ei}), \quad (1)$$

where y_{ei} is the ith datum for the eth earthquake, that is, y_{ei} is the geometric peak horizontal acceleration or the geometric mean response spectral value at a single period observed at a particular seismic station from the eth earthquake, and Z_{ei} is the Boore *et al.* (1997) prediction of that value, using their relation for strike-slip sources and shear velocities of 620 m/sec and 310 m/sec, respectively, for sites we classified as rock or soil. These shear velocities were based on the average velocities measured in boreholes (Boore and Joyner, 1997). For each period and site class (rock or soil), we used the maximum likelihood formalism of problem 1 in the Appendix to determine the mean value of Y, which we call the bias, and its standard deviation.

Figure 3 confirms that extensional regime motions are systematically lower than non-extensional regime motions. This figure shows that the relation of Boore *et al.* (1997) for strike-slip sources overpredicts (bias < 0) the extensional regime rock motions by two standard deviations or more at all periods, and this relation overpredicts the soil motions by more than two standard deviations for PGA and all periods

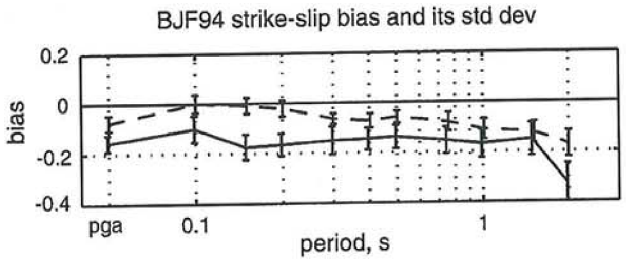

Figure 3. Bias of Boore *et al.* (1997) predicted strike-slip ground motions with respect to the extensional regime observations. Negative bias indicates that Boore relation overpredicts observations. Solid line, rock relation; dashed line, soil relation. Biases and standard errors were obtained using the Appendix.

tested except those in the 0.1–0.2 sec range. It must be recalled that the predicted motions depend on the appropriateness of the shear velocities (620 m/sec for rock and 310 m/sec for soil) assumed for our extensional regime sites. Our assumed velocity is probably fine for soil sites, but later we present data that suggest that the assumed rock velocity might be a little low, meaning that the relation by Boore *et al.* (1997) does not actually overpredict as much as Figure 3 indicates.

Regression of Ground Motions

We have developed new ground-motion prediction equations SEA99 for geometric mean horizontal PGA and 5% damped PSV from the extensional region strong-motion data set. This relation may be used in the 5.0–7.7 range of moment magnitude and the 0–100 km distance range for extensional regime ground motions. The general form of the regression relation is

$$\log_{10}(Z) = b_1 + b_2\,(\mathbf{M} - 6) + b_3\,(\mathbf{M} - 6)^2 + b_5 \log_{10} D + b_6\Gamma \quad (2)$$

where Z is peak horizontal acceleration (g) or pseudovelocity response (cm/sec) at 5% damping for the geometrical mean horizontal component of motion, $\mathbf{M}$ is moment magnitude (Hanks and Kanamori, 1979),

$$D = \sqrt{r_{jb}^2 + h^2}, \quad (3)$$

r_{jb} is the Joyner-Boore distance (see Abrahamson and Shedlock, 1997, Fig. 1), Γ is 0 for a rock site and is 1 for a soil site, and b_1, b_2, . . . , b_6, and h are regression coefficients that depend on period.

Because our data set does not include events of very large magnitude, the coefficients b_2 and b_3 cannot be determined directly from our data set in a way that gives reliable ground motion predictions when evaluated at large magnitude. Consequently, as in SEA96, we used the b_2 and b_3 coefficients determined from a larger data set by Boore *et al.* (1993). Unlike our practice in SEA96, however, we decided to use a soil coefficient b_6 derived from Boore *et al.* (1994, 1997), because their data set was larger than the extensional regime data set, and the site geologic characteristics were more well known in that study. Specifically, following Boore *et al.* (1994, equation 3) we used $b_6 = B_v\,(\log_{10} 310 - \log_{10} 620)$, where B_v was taken from Boore *et al.* (1997, Table 8), and where 310m/sec was the shear velocity used for sites we classified as soil and 620 m/sec was the shear velocity for sites classified as rock (Boore and Joyner, 1997).

Thus, we used our extensional regime data set to constrain the distance term b_5, the pseudodepth h, and the constant offset b_1. At each period we formed the residuals

$$\delta_i = \log_{10}(y_i) - b_2(\mathbf{M}_i - 6) - b_3\,(\mathbf{M}_i - 6)^2 - b_6\Gamma_i \quad (4)$$

where y_i is the ith ground motion datum (geometric mean horizontal PGA or PSV) in the extensional regime data set, $\mathbf{M}_i$ and Γ_i are the moment magnitude and site geology coefficient corresponding to the ith datum, respectively, b_2 and b_3 are the Boore *et al.* (1993) coefficients, and b_6 is derived as described previously. We then used the one-stage regression method of Joyner and Boore (1993, 1994) to fit the residuals by an equation of the form

$$\delta_i = b_1 + b_5 \log_{10}(D_i) \quad (5)$$

where b_1, b_5, and h were adjusted to fit the data (Table 2). The one-stage regression method was used rather than the two-stage method because our data set contained many earthquakes recorded by only a single station, and the two-stage method underestimates the earthquake-to-earthquake component of the variation in this situation. The resulting b_1, b_5, and h coefficients were smoothed by fitting cubic functions of period (Table 2).

The standard deviation of $\log_{10}(Z)$ is $\sigma_{\log Z}$, which is given by

$$\sigma_{\log Z} = \sqrt{\sigma_1^2 + \sigma_2^2}. \quad (6)$$

The terms σ_1 and σ_2 (Table 2) are the standard deviation of ε_r and ε_e (Boore *et al.*, 1993, equation 1), which are respectively the record-to-record variation and the earthquake-to-earthquake variation in the residuals. Note that Table 2 contains a column for σ_3, which is the component standard deviation (i.e., it is σ_c in Boore *et al.*, 1993, equation 3). The term σ_3 is not used to define the standard deviation of the geometric mean, but to form the standard deviation of the randomly oriented horizontal component, which is $\sigma_R = \sqrt{\sigma_1^2 + \sigma_2^2 + \sigma_3^2}$. The σ_1, σ_2, and σ_3 terms have been smoothed by fitting cubic functions of period. Sample evaluations of the SEA99 relationship are given in Table 3.

Table 2
Smoothed Coefficients for Regression Relation SEA99, for Geometric Mean Horizonal PGD and 5% damped PSV

Period (sec)	nr*	ne*	b_1	b_2	b_3	b_5	b_6	h (km)	σ_1	σ_2	σ_3
PGA	142	39	0.299	0.229	0	−1.052	0.112	7.27	0.172	0.108	0.094
0.100	131	38	2.144	0.327	−0.098	−1.250	0.064	9.99	0.205	0.181	0.110
0.110	132	38	2.155	0.318	−0.100	−1.207	0.064	9.84	0.205	0.168	0.111
0.120	132	38	2.165	0.313	−0.101	−1.173	0.065	9.69	0.204	0.156	0.113
0.130	132	38	2.174	0.309	−0.101	−1.145	0.067	9.54	0.205	0.146	0.114
0.140	132	38	2.183	0.307	−0.100	−1.122	0.069	9.39	0.205	0.137	0.115
0.150	132	38	2.191	0.305	−0.099	−1.103	0.072	9.25	0.205	0.129	0.116
0.160	132	38	2.199	0.305	−0.098	−1.088	0.075	9.12	0.206	0.122	0.117
0.170	132	38	2.206	0.305	−0.096	−1.075	0.078	8.99	0.207	0.116	0.118
0.180	132	38	2.212	0.306	−0.094	−1.064	0.081	8.86	0.208	0.110	0.119
0.190	132	38	2.218	0.308	−0.092	−1.055	0.085	8.74	0.209	0.105	0.119
0.200	132	38	2.224	0.309	−0.090	−1.047	0.088	8.63	0.210	0.100	0.120
0.220	132	38	2.234	0.313	−0.086	−1.036	0.095	8.41	0.212	0.092	0.121
0.240	132	38	2.242	0.318	−0.082	−1.029	0.102	8.22	0.214	0.086	0.122
0.260	132	38	2.250	0.323	−0.078	−1.024	0.108	8.04	0.216	0.081	0.123
0.280	132	38	2.257	0.329	−0.073	−1.021	0.115	7.87	0.218	0.076	0.124
0.300	132	38	2.263	0.334	−0.070	−1.020	0.121	7.72	0.220	0.073	0.125
0.320	132	38	2.268	0.340	−0.066	−1.019	0.126	7.58	0.221	0.070	0.126
0.340	132	38	2.272	0.345	−0.062	−1.020	0.132	7.45	0.223	0.067	0.126
0.360	132	38	2.276	0.350	−0.059	−1.021	0.137	7.33	0.225	0.065	0.127
0.380	132	38	2.279	0.356	−0.055	−1.023	0.142	7.22	0.227	0.064	0.128
0.400	132	38	2.282	0.361	−0.052	−1.025	0.147	7.11	0.228	0.063	0.128
0.420	132	38	2.285	0.365	−0.049	−1.027	0.151	7.02	0.230	0.062	0.129
0.440	132	38	2.287	0.370	−0.047	−1.030	0.155	6.93	0.231	0.061	0.129
0.460	132	38	2.289	0.375	−0.044	−1.032	0.159	6.85	0.233	0.061	0.129
0.480	132	38	2.291	0.379	−0.042	−1.035	0.163	6.77	0.234	0.060	0.130
0.500	132	38	2.292	0.384	−0.039	−1.038	0.166	6.70	0.235	0.061	0.130
0.550	132	38	2.294	0.394	−0.034	−1.044	0.174	6.55	0.238	0.061	0.131
0.600	132	38	2.295	0.403	−0.030	−1.051	0.181	6.42	0.241	0.063	0.132
0.650	132	38	2.295	0.411	−0.026	−1.057	0.187	6.32	0.243	0.065	0.132
0.700	132	38	2.294	0.418	−0.023	−1.062	0.192	6.23	0.245	0.068	0.133
0.750	132	38	2.292	0.425	−0.020	−1.067	0.197	6.17	0.247	0.071	0.133
0.800	132	38	2.290	0.431	−0.018	−1.071	0.200	6.11	0.249	0.074	0.134
0.850	131	38	2.287	0.437	−0.016	−1.075	0.203	6.07	0.250	0.077	0.134
0.900	131	38	2.284	0.442	−0.015	−1.078	0.206	6.04	0.251	0.081	0.134
0.950	131	38	2.280	0.446	−0.014	−1.081	0.208	6.02	0.253	0.085	0.135
1.000	131	38	2.276	0.450	−0.014	−1.083	0.210	6.01	0.254	0.089	0.135
1.100	119	35	2.267	0.457	−0.013	−1.085	0.213	6.01	0.255	0.097	0.135
1.200	116	35	2.258	0.462	−0.014	−1.086	0.214	6.03	0.257	0.106	0.136
1.300	116	35	2.248	0.466	−0.015	−1.085	0.214	6.07	0.258	0.115	0.136
1.400	114	34	2.237	0.469	−0.017	−1.083	0.213	6.13	0.258	0.123	0.136
1.500	114	34	2.226	0.471	−0.019	−1.079	0.212	6.21	0.259	0.132	0.137
1.600	114	34	2.215	0.472	−0.022	−1.075	0.210	6.29	0.259	0.141	0.137
1.700	105	34	2.203	0.473	−0.025	−1.070	0.207	6.39	0.259	0.150	0.137
1.800	105	34	2.192	0.472	−0.029	−1.063	0.204	6.49	0.259	0.158	0.137
1.900	105	34	2.180	0.472	−0.032	−1.056	0.201	6.60	0.258	0.167	0.137
2.000	105	34	2.168	0.471	−0.037	−1.049	0.197	6.71	0.258	0.175	0.137

*nr, number of records used; ne, number of earthquakes used.

Figure 4 shows that the ground motions predicted by the smoothed coefficients agree well with those predicted from the unsmoothed coefficients.

Evaluation of SEA99

To check SEA99 we wanted to determine whether its residuals for each period were unbiased and were independent of log-distance $\log_{10}(D)$ and moment magnitude **M**. We used the same definition of residual as defined in equation (1), except that Z_{ei} is the SEA99 prediction of the ground motion. For each period and site class (rock or soil), we used the maximum likelihood formalism of Problem 1 in the Appendix to determine the mean value of Y, which we call the bias, and its standard deviation. For each period and site class we used the maximum likelihood formalism of Problem 2 in the Appendix to determine the slope (and its error) of the maximum-likelihood straight line that best fits the residuals as a function of an independent variable. When the independent variable was $\log_{10}(D)$, we denoted the resulting

Table 3
Predicted Geometric Mean PGA, PSV and σ for SEA99 Evaluated Numerically for Selected Magnitudes, Distances, Periods, and Site Conditions

M	r_{jb} (km)	Site Geol	PGA (g)	PSV (cm/sec at 0.1 sec)	PSV (cm/sec at 0.5 sec)	PSV (cm/s at 2.0 sec)
5.5	0	rock	1.8974e−01	5.0880e+00	1.7092e+01	1.1377e+01
5.5	0	soil	2.4556e−01	5.8958e+00	2.5049e+01	1.7907e+01
5.5	70	rock	1.7418e−02	4.4071e−01	1.4893e+00	9.6752e−01
5.5	70	soil	2.2543e−02	5.1069e−01	2.1826e+00	1.5229e+00
6.5	0	rock	3.2149e−01	1.0803e+01	4.1379e+01	3.3653e+01
6.5	0	soil	4.1607e−01	1.2518e+01	6.0644e+01	5.2969e+01
6.5	70	rock	2.9513e−02	9.3574e−01	3.6056e+00	2.8619e+00
6.5	70	soil	3.8195e−02	1.0843e+00	5.2842e+00	4.5046e+00
7.5	0	rock	5.4471e−01	1.4606e+01	8.3711e+01	8.3949e+01
7.5	0	soil	7.0496e−01	1.6926e+01	1.2268e+02	1.3214e+02
7.5	70	rock	5.0004e−02	1.2652e+00	7.2943e+00	7.1393e+00
7.5	70	soil	6.4715e−02	1.4661e+00	1.0690e+01	1.1237e+01
σ_{logZ}			2.0310e−01	2.7347e−01	2.4279e−01	3.1175e−01
σ_R			2.2379e−01	2.9476e−01	2.7540e−01	3.4053e−01

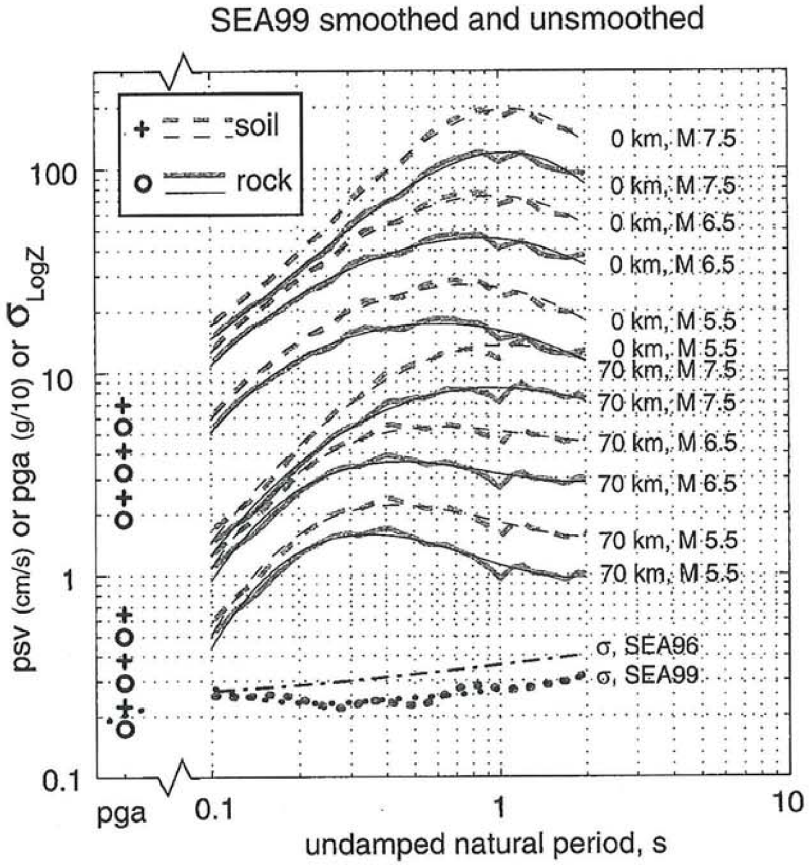

Figure 4. Summary of SEA99 geometric mean horizontal ground motions for M 5.5, 6.5, and 7.5, for distances 0 and 70 km, for rock and soil site conditions, and for smoothed and unsmoothed coefficients. Circles and + symbols indicate rock and soil PGA, respectively, in units of g/10, for sequence of distance and M shown on right of figure. Solid lines, rock sites; dashed lines, soil sites. Gray and black indicate SEA99 PSV using unsmoothed and smoothed coefficients, respectively. Dotted lines at bottom show smoothed and unsmoothed σ_{logZ} in units of Table 2 (i.e., not as multiplicative factor). Chained line shows σ_{logZ} for SEA96.

slope and its standard deviation by s_d and σ_d. When the independent variable was moment magnitude, we denoted the resulting slope and its standard deviation by s_m and σ_m.

Figure 5a shows that the bias (mean residual) of SEA99 is negligible for soil sites at all periods, but for rock sites SEA99 overestimates the data on the average by about 0.08 $\log_{10}$ units or about 20%. This discrepancy for rock motions exists because we have forced the difference between predicted rock and soil motions to equal the difference we derived from Boore *et al.* (1994, 1997). SEA99 fits the soil data better because we have far more soil data than rock data. The overprediction of rock motions by SEA99 is consistent with the hypothesis that the extensional regime rocks are systematically harder than the western U.S. rocks (most

of which come from coastal California) described by Boore *et al.* (1997), but we have no geologic reason to believe that this hypothesized difference in the rocks is true. Earlier we noted that the Boore *et al.* (1997) overpredictions for rock sites in Figure 3 might be biased by our use of 620 m/sec for rock shear velocity. If we use the SEA99 rock bias in Figure 5a as a correction of the rock curve in Figure 3, the corrected Boore *et al.* (1997) rock motions still overpredict the extensional regime data in the entire period band considered by 0.03 to 0.20 $\log_{10}$ units, reinforcing our earlier conclusion that extensional regime ground motions are lower than those in other tectonic regimes. This overprediction exceeds 2 standard deviations for PGA and for PSV in the 0.4–0.5 sec and 1.5–2.0 sec bands. Figure 5b shows that there is no systematic distance dependence in the residuals of SEA99, either for rock or soil sites. Slope s_d is essentially zero across the entire period band.

There is evidence of a magnitude dependence of the SEA99 residuals, which is not entirely surprising because in (2) and (4) we used the magnitude coefficients b_2 and b_3 determined from a different, larger data set Boore *et al.* (1997). Figure 6 shows the distribution of residuals as a function of magnitude for rock and soil for a single period, 2.0 sec. The maximum-likelihood line is dashed, and its slope is s_m. The magnitude dependence of SEA99 residuals is the worst for this period, for reasons explained subsequently. Figure 5c shows the slopes s_m for all periods for rock and soil sites. Positive s_m signifies that SEA99 underpredicts observed motions more at large magnitude than at small, as can be seen in the examples in Figure 6.

The two main characteristics of s_m (T) in Figure 5c are

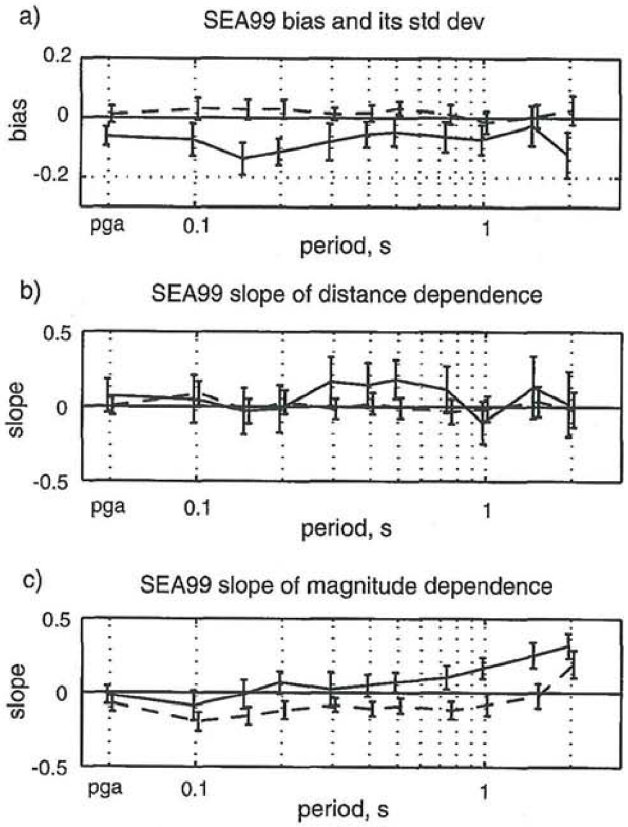

Figure 5. Bias and dependences of SEA99 residuals. Solid line, rock relation; dashed line, soil relation. Maximum likelihood values and standard errors obtained using Appendix. (a) Mean bias of residuals. (b) Slope of maximum likelihood line fit through residuals as a function of log10(distance). (c) Slope of maximum-likelihood line fit through residuals as a function of moment magnitude.

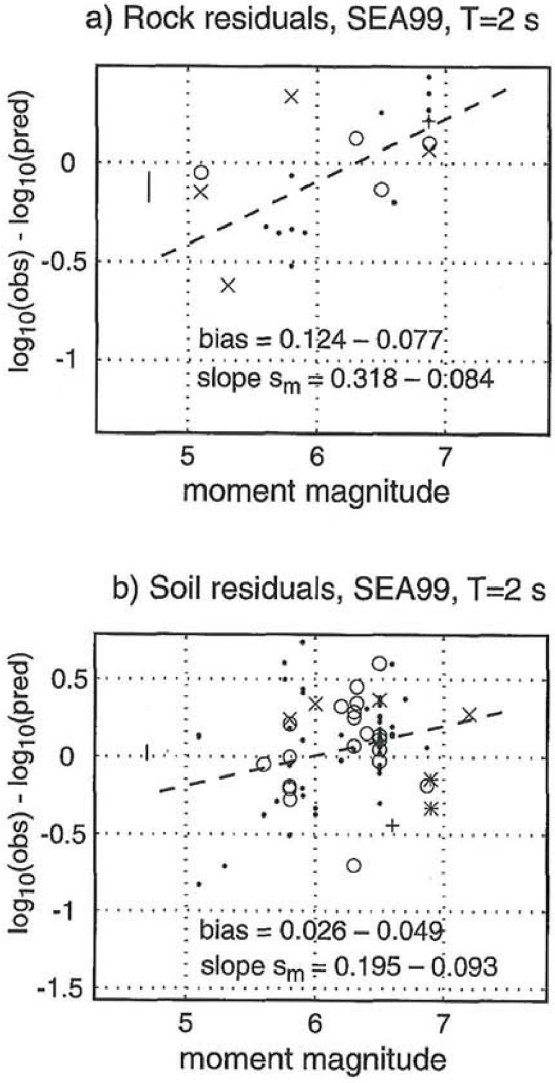

Figure 6. Dependence of SEA99 residuals on moment magnitude for a 2.0-sec period. Dashed line is maximum likelihood fit to points. Short vertical bar at M = 4.7 is mean bias ± standard error of mean. Symbol type indicates distance r_{jb}: dot, 0–20 km; circle, 20–40 km; ×, 40–60 km; +, 60–80 km; *, r_{jb} > 80 km. (a) Rock residuals. (b) Soil residuals.

that it is higher for rock residuals than for soil, and it tends to increase for longer periods. Both these characteristics are caused in part by the influence of a small number of data at high and low magnitude ends of the data set. Consider first the high value of s_m for rock sites at periods greater than 1.0 sec. All the rock data for $M > 6.7$ in Figure 6a are from a single earthquake, the 1980, M 6.87, Irpinia earthquake. This earthquake may simply have unusually strong motions at a 2.0-sec period, which would be a manifestation of the earthquake-to-earthquake variation captured in the parameter ε_e in our formulation. In other words, we expect that some earthquakes will be systematically high and others will be systematically low compared with SEA99; σ_2 quantifies this variability. When the Irpinia data are omitted from the calculation of s_m for rock sites, a slight magnitude dependence remains at 1.5 and 2.0 sec ($s_m = 0.237 \pm 0.153$ and 0.192 ± 0.153, respectively). All other periods for rock have no significant magnitude dependence. A similar sampling problem probably contributes to the low values of s_m (T) at short periods for soil sites. Figure 7 shows that at 0.1-sec period (and in the band 0.1–1.0 sec, not shown) the magnitude dependence is strongly affected by a few high residuals at small magnitudes. Consequently, we believe that the magnitude dependence of residuals in Figure 5c is in part caused by the sparseness of the SEA99 data set at high and low magnitudes.

Despite the large value of s_m at a 2.0-sec period for rock sites, there is no good reason to expect that SEA99 will systematically underpredict 2.0-sec rock motions at large magnitudes. Although extrapolation of the dashed line in Figure 6a to M 7–7.5 suggests that SEA99 would underpredict rock motions in this magnitude range by a factor of about 2, there is no physical reason to believe that the linear extrapolation of residuals in Figure 6a above M 7.0 is valid. The more plentiful soil residuals (Fig. 6b) do not suggest that the SEA99 magnitude dependence is significantly wrong or significantly biased at large magnitude, and the SEA99 magnitude dependence is constrained up to M 7.7 by data used by Boore *et al.* (1993, 1997).

Because the regression coefficients that we have determined are stochastic variables and are thus uncertain, the value of $\sigma_{\log Z}$ (equation 6), which does not contain the effects of uncertainty in the regression coefficients, is less than the total uncertainty of predicted ground motions (Toro *et al.*, 1997) by an amount we estimate to be about 10% on the average. This difference can be determined from a Monte-Carlo simulation like that of Joyner and Boore (1993, 1994). Rather than doing such a simulation, we have assumed that the results of Joyner and Boore's second Monte Carlo simulation using the one-stage method (1993, 1994, Table 4, created with a data set consisting of 65 records and 13 earthquakes) are comparable with the results that would be obtained from Monte-Carlo simulation of the SEA99 data set of 142 records and 38 earthquakes. The results in Joyner and Boore (1994, Table 4, bottom four rows) show that the standard deviations of the logarithm of the predicted motions

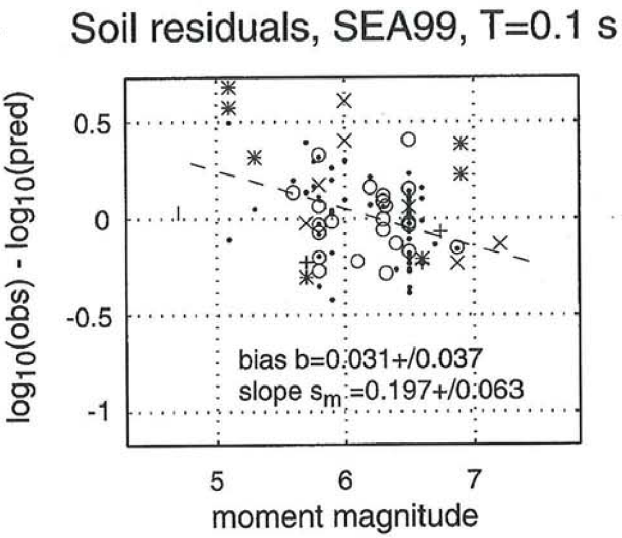

Figure 7. Dependence of SEA99 soil residuals on moment magnitude for a 0.1-sec period. Dashed line is maximum-likelihood fit to points. Short vertical bar at M = 4.7 is mean bias ± standard error of mean. Symbol type indicates distance r_{jb}: dot, 0–20 km; circle, 20–40 km; ×, 40–60 km; +, 60–80 km; *, r_{jb} > 80 km.

in their Monte-Carlo realizations were about 0.18 to 0.62 of their $\hat{\sigma} = \sqrt{\hat{\sigma}_r^2 + \hat{\sigma}_e^2}$ (see Joyner and Boore, 1994, for definition of these terms). Assuming these two sources of variance are uncorrelated so that their variances add, then $\sigma_{\log Z}$ is about 2–15% lower than the total uncertainty of predicted ground motions, the former percentage corresponding to well-sampled parts of the M-D space and the latter to poorly sampled parts.

Comparison with SEA96

In general, Figure 8 shows that SEA99 has motions that are as much as 20% higher than those of SEA96 at short distances (5–30 km), and SEA99's motions are about 20% lower than SEA96 at longer periods (1.0–2.0 sec) and larger distance (40–100 km). Because SEA99 and SEA96 have exactly the same magnitude dependence, the ratio of their motions is independent of magnitude. At zero distance, the SEA99 response spectra for rock and soil are about 0–15% lower than those of SEA96. SEA99 peak accelerations are similar to those of SEA96 for soil, and are 0–10% lower than SEA96 peak accelerations for rock. There is no obvious characteristic of the SEA99 data set that explains these differences with SEA96. The dispersion $\sigma_{\log Z}$ of SEA99 is considerably lower than that of SEA96 (Figure 4), probably because of our correction of errors in the data set.

Effect of SEA99 on Hazard Calculations

Compared with current hazard estimates (e.g., Frankel *et al.*, 1996), use of SEA99 for future hazard calculations at

sites in extensional regions will probably decrease estimates of seismic hazard by about 20% on the average, depending on proximity of the sites to source zones and depending on period. We estimate 20% by comparison of the SEA99 motions with those predicted by BJF94 (Boore *et al.*, 1994, 1997), which was one of the ground-motion-prediction relations used to develop the Frankel *et al.* (1996) hazard maps for the United States. Figure 9 shows a comparison of predicted PSV and PGA from SEA99 and BJF94. Because these two relations have the same magnitude dependence, their ratio is independent of magnitude. The BJF94 motions were calculated for the same source mechanism (strike-slip) and surface shear velocity (V_s = 760 m/sec) as are used in the Frankel *et al.* (1996) seismic hazard maps for the United States and the SEA99 motions were calculated for rock sites. In general SEA99 rock motions are lower than BJF94 motions, except for short distances at periods around 1.0 sec, where SEA99 motions exceed BJF94 motions by as much as 10%. It should be noted that a reasonable estimate of shear velocity at SEA99 rock sites is 620 m/sec (Boore and Joyner, 1997), which is lower than the 760 m/sec used in the U.S. national seismic hazard maps.

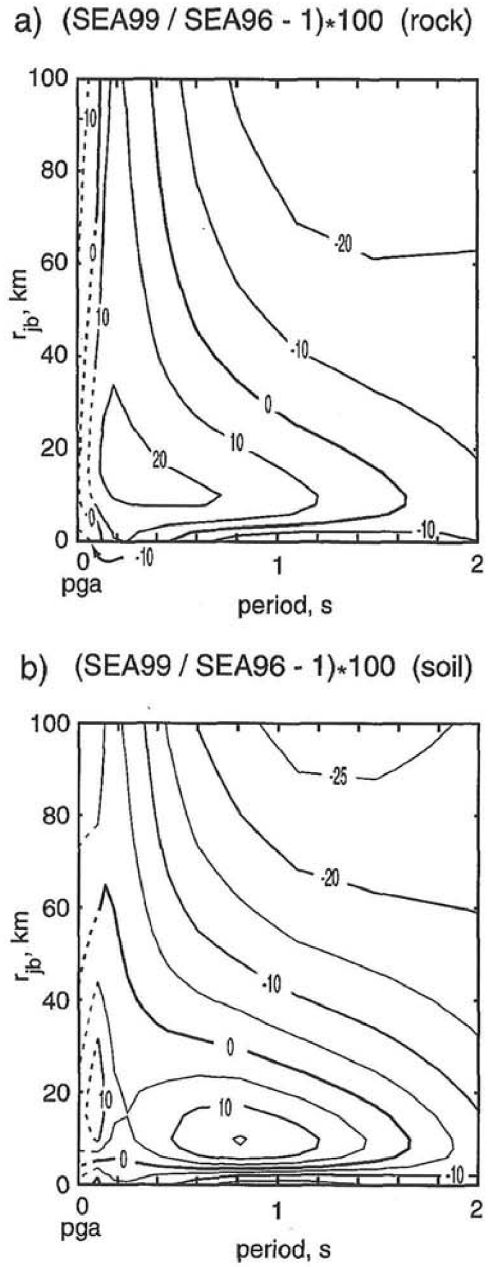

Figure 8. Ratio of SEA99 motions to SEA96 motions. Contours are expressed in percent and are dashed where interpolated between PGA results shown at 0.0 sec period and PSV results shown at periods greater or equal to 0.1 sec (a) Comparison for rock sites. (b) Comparison for soil sites.

Comparison of Ground Motions between Normal and Strike-Slip Earthquakes in Extensional Regions

Horizontal ground motions from extensional regime strike-slip earthquakes in our data set tend to be slightly larger than horizontal ground motions from normal-faulting earthquakes, but the difference is small and not significant. This contradicts our previously determined result in Spudich *et al.* (1996). To obtain our current results we divided our data set into normal-faulting earthquakes and strike-slip earthquakes based on their rake; earthquakes with slip di-

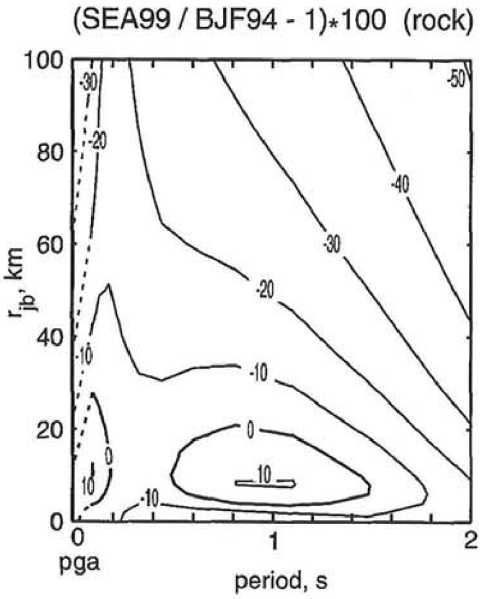

Figure 9. Ratio of SEA99 motions on rock sites to BJF94 motions calculated for strike-slip mechanism at sites having V_s = 760 m/sec, the site condition used in U.S. seismic hazard maps. Contours are expressed in percent and are dashed where interpolated between PGA results shown at 0.0 sec period and PSV results shown at periods greater or equal to 0.1 sec.

rections more than 45° away from horizontal (measured in the fault plane) were classified as normal mechanisms, and the remainder were classified as strike-slip mechanisms. For each record, we calculated its geometric mean PGA and PSV at the periods listed in Table 2. We then calculated the residuals Y_{ei} (equation 1) for the PGA and PSV observations for each record. We used the maximum-likelihood method in problem 1 of the Appendix to determine the mean residual and its standard deviation for each period and mechanism. Let $\hat{B}_{ss}(T)$ and $\hat{B}_{nl}(T)$ be the mean residuals as functions of period for strike-slip and normal events, and let $\hat{\sigma}_{Bs}(T)$ and $\hat{\sigma}_{Bn}(T)$ be the standard deviations of the means for the two mechanisms. Our null hypothesis is that the mean residuals for both mechanisms are the same. For each period we then ask the probability of observing a difference of mean residuals greater than or equal to $\Delta(T) = |\hat{B}_{ss}(T) - \hat{B}_{nl}(T)|$ if the null hypothesis is true and if our errors of observation of the strike-slip and normal mean residuals are Gaussian distributed with standard deviations $\hat{\sigma}_{Bs}(T)$ and $\hat{\sigma}_{Bn}(T)$, respectively. For each period the difference of mean residuals will be Gaussian distributed with variance $\hat{\sigma}^2_{Bs} + \hat{\sigma}^2_{Bn}$ and our desired probability is the area of the Gaussian having difference greater than Δ. Figure 10 shows that the ratio of strike-slip to normal motions, which is calculated as $10^{[\hat{B}_{ss}(T) - \hat{B}_{nl}(T)]}$, ranges from about 1.0 to 1.4, but only at short and long periods might the difference be significant (i.e., unlikely to result from the null hypothesis).

Despite the fact that extensional regime strike-slip motions exceed normal motions at all periods, a comparison of normal and strike-slip residual that lumps all periods together shows that extensional regime strike-slip motions are not significantly larger than normal motions. We performed this comparison as follows. We could not perform this broadband comparison directly on the results in Figure 10 because they are correlated from period to period because of the cubic smoothing of regression coefficients and owing to the bandwidth of the response spectral oscillators. Also, the number of residuals varies as a function of period. We performed the broadband comparison by recalculating the normal and strike-slip residuals using unsmoothed regression coefficients and by applying the method of Problem 1 in the Appendix to a subset of residuals consisting of peak acceleration residuals and PSV residuals at 7 periods, chosen to minimize overlap of oscillator response, in the 0.11 sec to 0.80 sec band. This particular choice of PGA and PSV data yielded a completely homogeneous data set (i.e., exactly the same earthquakes and stations at all periods, after excluding the PGA residuals from the Irpinia 40-s aftershock, for which there were no PSV residuals). Over this period band, the mean extensional regime strike-slip motion is 1.09 times larger than the mean normal motion, but the probability of observing a difference of mean residuals equaling or exceeding this observed difference if the null hypothesis is true is about 0.42. Thus, we cannot reject the null hypothesis.

Our observation that normal-faulting horizontal motions are not significantly different from extensional regime strike-slip motions should be subject to additional verification. Note that we have examined the residual with respect to an assumed "correct" predictive relation, taken to be the SEA99 relation. In a prior version of this comparison using the SEA96 data set, Spudich *et al.* (1996) found that it was possible to find that normal-faulting ground motions were either smaller or larger than strike-slip ground motions, depending on the predictive relation used as the basis. We believe that SEA99 is the most appropriate predictive relation to use because it was derived from our data set.

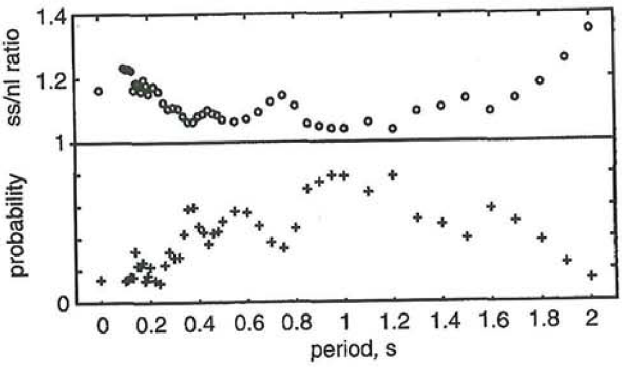

Figure 10. Comparison of mean ground motions for extensional regime strike-slip and normal faulting earthquakes as a function of period. The PGA is shown at zero period, and PSV is shown at other periods. Upper panel, ratio of mean strike-slip to mean normal motions; lower panel, probability that a ratio equaling or exceeding that shown in the upper panel could be obtained from the null hypothesis that the strike-slip to normal ratio is equal to unity.

Our observation of the similarity of normal motions and extensional regime strike-slip motions contradicts the laboratory results of Brune and Anooshehpoor (1999), who showed that strike-slip slip events in a foam rubber model generated much larger motions than normal events. The discrepancy between our results and their results might be caused by the fact that the laboratory strike-slip fault did not have a weak zone near the surface (R. Anooshehpoor, personal communication). Our result is also surprising in light of the observation by Becker and Abrahamson (1998) that normal stress drops are 10–25% lower than strike-slip stress drops in the SEA96 data set. Becker and Abrahamson's result contradicts McGarr's (1984) hypothesis that the stress drops of both these mechanisms in extensional regimes should be similar to each other but less than stress drops of compressional or intermediate regimes.

Our results imply that ground motions from strike-slip earthquakes in extensional regimes might be systematically less than ground motions of strike-slip earthquakes in other stress regimes. In addition, because strike-slip earthquakes can occur in extensional, intermediate, and compressive stress regimes, it might be that the style-of-faulting factor, which characterizes the effect of source mechanism on ground motion, may be insufficient to characterize the ef-

fects of stress regime. These implications should be confirmed observationally.

Acknowledgments

We thank the many people who contributed to this work. Seismic data and site information were contributed by N. Ambraseys, E. Carro, M. Çelebi, R. Darraugh, D. Rinaldis, J. Gomberg, M. Henger, E. Inan, S. Jackson, G. McVerry, H. Meidow, R. Pelzing, A. Rovelli, G. Shamir, A. Shapiro, R. B. Smith, L. Valensise, and R. Westaway. F. Sabetta found the errors in our locations of Italian earthquakes. G. Atkinson and G. Toro provided reviews that led to significant improvement of the manuscript.

References

Abrahamson, N. A., and K. M. Shedlock (1997). Overview, *Seism. Res. Lett.* **68,** 9–23.

Abrahamson, N. A., and W. J. Silva (1997). Empirical response spectral attenuation relations for shallow crustal earthquakes, *Seism. Res. Lett.* **68,** 94–109.

Becker, A. M., and N. A. Abrahamson (1998). Stress drops in extensional regimes, *Seism. Res. Lett.* **69,** 172.

Boore, D. M., and W. B. Joyner (1997). Site amplifications for generic rock sites, *Bull. Seism. Soc. Am.* **87,** 327–341.

Boore, D. M., W. B. Joyner, and T. E. Fumal (1993). Estimation of response spectra and peak accelerations from western North American earthquakes: an interim report, *U.S. Geol. Surv. Open-File Rep. 93-509,* 72 pp.

Boore, D. M., W. B. Joyner, and T. E. Fumal (1994). Estimation of response spectra and peak accelerations from western North American earthquakes: an interim report, Part 2, *U.S. Geol. Surv. Open-File Rep. 94-127,* 40 pp.

Boore, D. M., W. B. Joyner, and T. E. Fumal (1997). Equations for estimating horizontal response spectra and peak acceleration from western North American earthquakes: a summary of recent work, *Seism. Res. Lett.* **68,** 128–153.

Brune, J., and A. Anooshehpoor (1999). Dynamic geometrical effects on strong ground motion in a normal fault model, *J. Geophys. Res.* **104,** 809–815.

Campbell, K. C. (1997). Empirical near-source attenuation relationships for horizontal and vertical components of peak ground acceleration, peak ground velocity, and pseudo-absolute acceleration response spectra, *Seism. Res. Let.* **68,** 154–179.

Christensen, N., and W. D. Mooney (1995). Seismic velocity structure and composition of the continental crust: a global view, *J. Geophys. Res.* **100,** 9761–9788.

Clarke, P. J., D. Paradissis, P. Briole, P. C. England, B. E. Parsons, H. Billiris, G. Veis, and J. C. Ruegg (1997). Geodetic investigation of the 13 May 1995 Kozani-Grevena (Greece) earthquake, *Geophys. Res. Lett.* **24,** 707–710.

Cocco, M., and F. Pacor (1993). The rupture process of the 1980 Irpinia, Italy, earthquake from the inversion of strong motion waveforms, *Tectonophys.* **218,** 157–177.

Durukal, E., M. Erdik, J. Avci, Ö. Yüzügüllü, Y. Alpay, B. Avar, C. Zülfikar, T. Biro, and A. Mert (1998). Analysis of the strong motion data of the 1995 Dinar, Turkey earthquake, *Soil Dyn. Earthquake Eng.* **17,** 557–578.

Erdik, M., and E. Durukal (1997). Analysis of the strong motion data associated with the 1995 Dinar (Turkey) earthquake, (abstract with programs) Western States Seismic Policy Council Basin and Range Seismic Hazards Summit, May 12–15, 1997, Reno, NV.

Frankel, A., C. Mueller, T. Barnhard, D. Perkins, E. V. Leyendecker, N. Dickman, S. Hanson, and M. Hopper (1996). National Seismic Hazard Maps: Documentation June 1996, *U.S. Geological Survey Open File Report 96–532,* 110 pp.

Fuenzalida, H., L. Dorbath, A. Cisternas, H. Eyidogan, A. Barka, L. Rivera, H. Haessler, H. Philip, and N. Lyberis (1997). Mechanism of the 1992 Erzincan earthquake and its aftershocks, tectonics of the Erzincan basin, and decoupling on the North Anatolian Fault, *Geophys. J. Int.* **129,** 1–28.

Hanks, T. C., and H. Kanamori (1979). A moment-magnitude scale, *J. Geophys. Res.* **84,** 2348–2350.

Hillel, W. (1997). The November 22, 1995 Nuweiba earthquake, Gulf of Elat (Aqaba); post-seismic analysis of failure features and seismic hazard implications, report for the Geol. Surv. of Israel, Jerusalem, 58 pp.

Joyner, W. B., and D. M. Boore (1981). Peak horizontal acceleration and velocity from strong-motion records including records from the 1979 Imperial Valley, California, earthquake, *Bull. Seism. Soc. Am.* **71,** 2011–2038.

Joyner, W. B., and D. M. Boore (1988). Measurement, characterization, and prediction of strong ground motion, *Proc. Earthquake Eng. Soil Dynamics II,* GT Div/ASCE, Park City, UT, 27–June.

Joyner, W. B., and D. M. Boore (1993). Methods for regression analysis of strong-motion data, *Bull. Seism. Soc. Am.* **83,** 469–487.

Joyner, W. B., and D. M. Boore (1994). Errata: methods for regression analysis of strong-motion data, *Bull. Seism. Soc. Am.* **84,** 955–956.

Lum, P. K., and K. K. Honda (undated). Processed seismic motion records from Little Skull Mountain, Nevada, earthquake recorded at stations in southern Nevada, Report JAB-10733-TM6, URS/John A. Blume & Associates, San Francisco, CA, 180 pp.

McGarr, A. (1984). Scaling of ground-motion parameters, state of stress, and focal depth, *J. Geophys. Res.* **89,** 6969–6979.

Menke, W. (1984). Geophysical Data Analysis: Discrete Inverse Theory, Academic Press, Orlando, FL, 260 pp.

Oglesby, D., R. Archuleta, and S. Nielsen (1998). Earthquakes on dipping faults: the effects of broken symmetry, *Science* **280,** 1055–1059.

Papazachos, B. C., D. G. Panagiotopoulos, E. M. Scordilis, G. F. Karakaisis, Ch. A. Papaioannou, B. G. Karakostas, E. E. Papadimitriou, A. A. Kiratzi, P. M. Hatzidimitriou, G. N. Leventakis, Ph. S. Voidomatis, K. I. Peftitselis, and T. M. Tsapanos (1995). Focal properties of the 13 May 1995 large (M_s = 6.6) earthquake in the Kozani area (North Greece), *Geophys. Lab. Aristotle Univ.,* Publ. No. 4, 1–13.

Sadigh, K., C. Y. Chang, J. A. Egan, F. Makdisi, and R. R. Youngs (1997). Attenuation relationships for shallow crustal earthquakes based on California strong-motion data, *Seism. Res. Lett.* **68,** 180–189.

Shamir, G. (1996). Mechanics of earthquake rupture in fault step zones: the M_w = 7.1 Nuweiba earthquake, Gulf of Elat (Aqaba), 22 November 1995, *EOS Trans. Am. Geophys. Un.* (S) **77,** 501.

Spudich, P., J. Fletcher, M. Hellweg, J. Boatwright, C. Sullivan, W. B. Joyner, T. C. Hanks, D. M. Boore, A. F. McGarr, L. M. Baker, and A. G. Lindh (1996). Earthquake ground motions in extensional tectonic regimes, *U.S. Geological Survey Open-File Report 96–292,* 351 pp.

Spudich, P., J. Fletcher, M. Hellweg, J. Boatwright, C. Sullivan, W. B. Joyner, T. C. Hanks, D. M. Boore, A. F. McGarr, L. M. Baker, and A. G. Lindh (1997). SEA96: a new predictive relation for earthquake ground motions in extensional tectonic regimes, *Seism. Res. Lett.* **68,** 190–198.

Toro, G. R., N. A. Abrahamson, and J. F. Schneider (1997). Model of strong ground motions from earthquakes in central and eastern North America: best estimates and uncertainties, *Seism. Res. Lett.* **68,** 41–57.

Appendix

Maximum Likelihood Determination of Means, Slopes, and Intercepts

We adapted the maximum likelihood method of Joyner and Boore (1993, equations 5–16) to the problem of finding

mean values and linear relations that best fit experimental data sets. We refer to their equations when possible for brevity, and we adopt their notation except to suppress their use of boldface characters for vectors and matrices. We refer to equation n of Joyner and Boore (1993) as JB-n.

We seek to solve two problems to determine the characteristics of the residuals Y defined in (1). Problem 1: What are the mean value of Y and its standard deviation, taken over a desired subset of the residuals? Problem 2: What are the slope and standard deviation of the slope of the best-fitting line fit through a subset of the residuals as a function of M or $\log_{10}(D)$?

These problems are nontrivial because the errors in the residuals are correlated for each earthquake. Specifically, suppose that the eth earthquake has R_e data for a chosen period. We form column vector Y by grouping together all data from each earthquake for the selected period,

$$Y = [Y_{11}\ Y_{12} \ldots Y_{1R_1}\ Y_{21} \ldots Y_{2R_2} \ldots Y_{E\,R_E}]^T,$$

where E is the total number of earthquakes. Let N be the total number elements of Y. Our two problems can both be expressed as the linear system JB-5, $Y = XB + e$. For both problems e is an $N \times 1$ vector of errors. We assume the same error model as that of Joyner and Boore (1993). Let e_{ej} be the element of e corresponding to Y_{ej}. Error $e_{ej} = \varepsilon_e + \varepsilon_r$, where ε_e is an independent random variable that takes on a specific value for each earthquake, and ε_r is an independent random variable that takes on a specific value for each record. The means of ε_e and ε_r are both zero, and their variances are σ_e^2 and σ_r^2, respectively. Neither σ_e^2 nor σ_r^2 is known *a priori,* and they must be determined. The covariance matrix of e is V, given by JB-9-11.

For problem 1, X is an $N \times 1$ vector of ones, and B is simply a scalar, the desired mean value. For problem 2, X is an $N \times 2$ matrix, and $B = [b\ s]^T$, where s is the slope and b is the intercept of the desired best-fitting line. The first column of X is a vector of ones, and the second column of X is a column of independent variables [moment magnitudes M or log-distances $\log_{10}(D)$] corresponding to each element of Y.

For both problems, the solution for B is $\hat{B}(\gamma)$ given by JB-12, where γ is an unknown parameter between 0 and 1. Typically we found γ_o, the maximum likelihood γ, by evaluating JB-12, JB-15, and JB-14 on a densely sampled grid of trial γ values and choosing the value of γ that maximized the likelihood function JB-14. After γ_o is determined, we obtain σ_e^2 and σ_r^2 from γ_o as described below.

Problems 1 and 2 were handled differently. For problem 2, the results were obtained purely numerically, but problem 1 was sufficiently simple that we could perform most of the needed matrix multiplications and inversions analytically.

Problem 1

The solution of problem 1 for the mean value of the residuals is $\hat{B}(\gamma_o) = q^T W(\gamma_o)$, where $W(\gamma_o) = F(\gamma_o)/(P^T F(\gamma_o))$, $q^T = [q_1\ q_2 \cdots q_E]$, $P^T = [R_1\ R_2 \cdots R_E]$, $F = [F_1\ F_2 \cdots F_E]^T$, $F_i = (1 - \gamma_o)/D_i$, $D_i = 1 - (R_i - 1)\gamma_o^2 + (R_i - 2)\gamma_o$, and $q_e = \sum_{i=1}^{R_e} Y_{ei}$. This result is obtained by inserting the expressions in Joyner and Boore (1993) Appendix B, especially JB-B2, B3, and B8, into JB-12. Then the variance of the mean value $\hat{B}(\gamma_o)$ is given by $\mathrm{var}(\hat{B}(\gamma_o)) = \sum_{i=1}^{E} W_i^2(\gamma_o)\mathrm{var}(q_i)$, and $\mathrm{var}(q_i) = R_i\sigma_r^2 + R_i^2\sigma_e^2$. We obtain $\hat{\sigma}^2$ from JB-16, except that we substitute the denominator $(N - 1)$ for the $(N - 4)$ in JB-16 because problem 1 has only a single degree of freedom. Variance $\sigma_e^2 = \gamma\hat{\sigma}^2$, and $\sigma_r^2 = \hat{\sigma}^2 - \sigma_e^2$. The optimum value γ_o of γ is chosen as described earlier. In the main body of the paper $\hat{B}(\gamma_o)$ is called the bias, and $\hat{\sigma}_B = \sqrt{\mathrm{var}(\hat{B}(\gamma_o))}$ is its standard deviation.

Problem 2

This problem is solved entirely numerically. If we define $T = X^T v^{-1} X$ and $U = X^T v^{-1} Y$, then from JB-12 we can derive $T\hat{B} = U$. This equation is solved for $\hat{B}$ using a QR decomposition. The matrix v^{-1} and the determinant $|v|$ are obtained using JB Appendix B. We obtain $\hat{\sigma}^2$ from JB-16, except that we substitute the denominator (N − 2) for the (N − 4) in JB-16 because problem 2 has only two degrees of freedom. Covariance matrix V is derived from $V = \hat{\sigma}^2 v$, which is slightly modified from JB-9. The covariance matrix of the $\hat{B}$ vector is given by $C = M^T V M$ (Menke, 1984, p. 58), where $M = T^{-1}X^T v^{-1}$. All these expressions are evaluated for the maximum likelihood γ_o chosen as described earlier. The slopes s_d and s_m in the main body of the paper are the second element of $\hat{B}$, and their standard deviations σ_d and σ_m are $\sqrt{C(2,2)}$.

U.S. Geological Survey
Mail Stop 977, 345 Middlefield Road
Menlo Park, CA 94025 USA
(P.S., W.B.J., A.G.L., D.M.B., J.B.F.)

Institute of Engineering Seismology and Earthquake Engineering (ITSAK)
46 Georgikis Scholis St.
Thessaloniki, Greece
(B.M.M.)

Manuscript received 1 May 1998.